A Two-Column Model Parameterization for Subgrid Surface Heterogeneity Driven Circulations

T. Waterman[1], A.D. Bragg[1], F. Hay-Chapman[2], P.A. Dirmeyer[2], M.D. Fowler[3], J. Simon[1], N. Chaney[1]

[1]Department of Civil and Environmental Engineering, Duke University Pratt School of Engineering, Durham, NC USA
[2]Atmospheric, Oceanic and Earth Sciences Department, George Mason University, Fairfax, VA USA
[3]National Center for Atmospheric Research (NCAR), Boulder, CO USA

Key Points:

- A parameterized circulation between two otherwise independent columns is described and evaluated for three simulation days
- Large-eddy simulations (LES) show substantial agreement with the overall circulation model structure proposed
- When implemented, the parameterized circulation yields similar changes in the atmospheric profiles and cloud production to LES

Corresponding author: Tyler Waterman, `tyler.waterman@duke.edu`

Abstract

Earth system models currently struggle to account for the complex effects that land surface heterogeneity can have on land-atmosphere interactions. Subgrid land surface heterogeneity is currently not well accounted for in land-atmosphere interactions in earth system models. There have been attempts to include the impact of this heterogeneity on the atmosphere, but they ignore the development of coherent secondary circulations that can be driven by spatial differential surface heating. A wealth of literature, particularly large-eddy simulation (LES) based studies, shows that these circulations have significant impacts on the development and organization of clouds. In this work, we describe a two-column model with a parameterized circulation driven by atmospheric virtual potential temperature profiles, differences in near surface temperature between the two columns, patterns of surface heterogeneity, and the mean background wind. Key aspects of the proposed model structure are compared with LES output, and the model is then implemented between two otherwise independent single column models. While some avenues for improvement exist, when the circulations are parameterized, we see increased cloud development and realistic changes to the mean profiles of temperature and moisture. The proposed model qualitatively matches expectations from the literature and LES, and points to the potential success of its future implementation in coarse grid models.

Plain Language Summary

This work addresses the challenge of incorporating land surface heterogeneity into earth system models to better understand land-atmosphere interactions. Current models struggle to account for the complex effects of subgrid land surface heterogeneity on these interactions, especially when a warmer region near a cooler region can cause a circulation to occur. The study proposes a two-column model that includes a parameterized circulation driven by vertical temperature profiles, surface temperature differences, surface heterogeneity patterns, and the background wind. The model is compared to high resolution large-eddy simulation (LES) output for three days in the Southern Great Plains. The results show that the model qualitatively reproduces patterns observed in LES and the existing literature, primarily that cloud production increases and concentrates over warmer surface areas. The model's success suggests its potential implementation in coarse grid models to explore regional and global atmospheric impacts of subgrid land surface heterogeneity. Additionally, the similarities between land surface heterogeneity circulations and other thermally driven circulations indicate potential applicability in subgrid-scale parameterization of sea and lake breezes. While limitations and opportunities for improvement exist, overall this work represents a promising step toward understanding the impacts of subgrid heterogeneity on cloud production and atmospheric processes in earth system models.

1 Introduction

Adequately understanding and modeling the coupling and feedbacks that occur between the land surface and the atmosphere has been a critical endeavor in the earth sciences for decades. When relying on coarse scale Earth system models (ESMs) to assess our global resilience to a changing climate, this issue becomes even more pronounced as fewer processes can be resolved and more must be parameterized. Local land-atmosphere influences on convection and cloud development are complex and challenging to parameterize (Santanello et al., 2018). Effectively including land-atmosphere interactions, however, is important as clouds remain one of the largest sources of uncertainties in predicting the extent and impact of climate change (Vial et al., 2013). A significant driver of these uncertainties over land is land surface heterogeneity, which is often poorly represented in coarse ESMs. Local-scale (kilometer-scale) spatial variations in surface properties inevitably affect state variables, such as soil moisture and temperature, and sur-

face fluxes of heat and moisture (Chaney et al., 2015), increasing their complexity and influencing the behavior of the larger scale water and energy cycles. When the variability and length scales of heterogeneity are significant, the resulting differential in surface heating and fluxes can cause secondary mesoscale circulations to occur, with potential ramifications for the boundary layer and cloud dynamics. Without modeling the impacts that these subgrid circulations have on the broader atmosphere, an often significant portion of the land-atmosphere coupling is ignored.

There is an extensive history of modeling studies with large-eddy simulation (LES) that show that surface heterogeneity induced secondary circulations at length scales significantly smaller than that of an ESM grid have important impacts on the atmosphere and cloud dynamics through secondary circulations (Stoll et al., 2020). These circulations are caused by pressure differences induced by temperature gradients near the surface, in many ways similar to the extensively studied sea breezes (Miller et al., 2003); flow converges over high temperature (and lower density) regions initiating a vertical transport which enhances an inverse temperature gradient in the upper region of the circulation, from which the flow diverges and then descends, completing a coherent circulation (Rochetin et al., 2017). Studies over both idealized surfaces (Hadfield et al., 1991; Avissar & Liu, 1996; Lee et al., 2019; Han et al., 2019) and those with realistic surface heterogeneity (Weaver, 2004; Garcia-Carreras et al., 2011; J. S. Simon et al., 2021) show that these circulations yield significant increases in cloud production as a result of the transport of moisture from near the surface to the top of the boundary layer. Under favorable conditions, they can also initiate deep convection or change the timing and spatial patterns of convective initiation (Kang & Ryu, 2016).

While there are many LES studies examining this phenomenon, the ability to represent it in the context of an ESM is limited. Atmospheric parameterizations capable of encoding a degree of atmospheric sub-grid variability, including the Cloud Layers Unified by Binormals (CLUBB) (Golaz et al., 2002) and Eddy Diffusivity Mass Flux (EDMF) (Sušelj et al., 2013), are increasingly being used in ESMs. Significant subgrid land surface heterogeneity is also already captured in land surface models (LSMs) through the use of tiling schemes which generate varying characteristics for multiple representative subgrid tiles (Bonan et al., 2002; Ducharne et al., 2000; Chaney et al., 2018). In ESMs, however, the tile surface fluxes and surface boundary conditions are averaged out when coupled to the atmosphere and higher order statistics (e.g. variances) are lost in the coupling, limiting any effective parameterization of sub-grid heterogeneity driven circulations. State of the art models have recently begun to account for inter-tile variations in the form of more accurate temperature and moisture variances (Huang et al., 2022), although the impacts on the atmosphere are not as significant as would be expected based on LES studies.

Some studies, mostly over the ocean rather than the land, have examined thermally driven circulations in the context of more simplistic models. A number of two-column models have been applied in this ocean context. (Nilsson & Emanuel, 1999; Raymond & Zeng, 2000; Naumann et al., 2017; Nuijens & Emanuel, 2018). These models also often rely on solving a more complex system of equations, increasing computation requirements and preventing ready implementation in the ESM sub-grid. A simpler two-column parameterization driven by sea surface temperature differences has been tested in this ocean context that performs fairly well (Naumann et al., 2019), but such a model has yet to be applied over the land. Despite the different setting and some challenges, these models show significantly different behavior than the coarse grid parameterizations in the ocean context (Nuijens & Emanuel, 2018) and indicate the potential of the two-column setup.

Any computationally efficient subgrid parameterization scheme will need to reflect the expected characteristics of heterogeneity-driven circulations and their impacts on the atmosphere found in the literature. Key characteristics include: **(i)** The flow velocity and

cloud impact of circulations are positively correlated with both the length-scale (or structure) of the surface heterogeneity and the variance of the surface heating (Kang & Ryu, 2016; Kang & Bryan, 2011; Lee et al., 2019; Avissar & Schmidt, 1998; Han et al., 2019; van Heerwaarden et al., 2014; Zhang et al., 2023; Margairaz et al., 2020), a phenomenon also seen in sea-breeze and lake-breeze literature (Crosman & Horel, 2010). **(ii)** There is some minimum length scale of heterogeneity necessary to see large scale impact. This exact scale is unclear, but is complex and on the order of the boundary layer height (Lee et al., 2019; van Heerwaarden et al., 2014; Margairaz et al., 2020). **(iii)** A background wind can reduce or completely wipe out a circulation, especially when oriented parallel to the temperature gradient, due to shear tearing the circulation apart or the wind preventing the air from forming a significant gradient. (Rochetin et al., 2017; Maronga & Raasch, 2013; Eder et al., 2015; Weaver, 2004; Avissar & Schmidt, 1998; Raasch & Harbusch, 2001). There is uncertainty around the magnitude of the velocity reduction from a zero background wind case. A 1:1 reduction has been suggested (Lee et al., 2019), however in the context of sea breezes a less significant reduction has been identified (Miller et al., 2003). **(iv)** Enhanced convection and cloud formation occurs primarily over the warmer regions, and convection is suppressed over the cooler regions (Taylor et al., 2012; J. S. Simon et al., 2021; Garcia-Carreras et al., 2011). This also results in the boundary layer height and vertical extent of the circulation being larger over the warm region than the cool region (Lee et al., 2019; Rochetin et al., 2017). **(v)** Horizontal circulation or breeze velocities up to 4 or $5m\ s^{-1}$ (Lee et al., 2019; Rochetin et al., 2017; Han et al., 2019) and vertical velocities of less than $1m\ s^{-1}$ (Garcia-Carreras et al., 2011; Maronga & Raasch, 2013). This will vary depending on a variety of conditions such as those described above, but provides a range of reasonable values.

Parameterizing heterogeneity induced secondary circulations in a computationally efficient manner that maintains the expected impacts and characteristics reported in the literature can offer critical improvements in the modeling of convective cloud development in coarse grid models. The focus of model development is to define it in such a way that it can be tuned to high resolution LES results, matching our expectations from the literature, functioning under the constraints of existing ESMs, and minimizing computational expense. Such a model may yield significant improvements in our coupling of the land and atmosphere at the coarse, ESM scale and aid in our understanding of these hard to observe phenomena. To achieve these results, we propose a simple two-column circulation model, where two independent atmospheric columns are coupled by a parameterized circulation driven by surface heating heterogeneity, and vertical temperature and density profiles.

2 Model Description

The approach to parameterizing circulations, described as follows, relies on the assumption that circulations are controlled by density differences between two otherwise largely independent atmospheric columns and the vertical profiles of density within these columns. One of these columns is forced with a warm (high sensible heat flux) surface while another is forced with a cool (low sensible heat flux) surface. The following section discusses the conceptual core of this model.

2.1 Circulation Velocity

To model the density induced flow between two atmospheric columns, we consider the advection-diffusion equation to model the transport of a species λ:

$$\delta_t \lambda + \nabla \cdot (\mathbf{V}\lambda) = \nabla\nabla : (\boldsymbol{\mathcal{D}}\lambda), \tag{1}$$

with advection velocity $\mathbf{V}$ and diffusion tensor $\boldsymbol{\mathcal{D}}$. We assume that this transport is primarily driven by advection, $\nabla \cdot (\mathbf{V}\lambda) >> \nabla\nabla : (\boldsymbol{\mathcal{D}}\lambda)$, and neglect the diffusion term.

We will model the advection velocity as

$$\mathbf{V}(z) = \mathbf{u_b}(z) + \mathbf{u_R}(z), \tag{2}$$

where $\mathbf{u_b}(z)$ is the background wind velocity in the absence of the circulation and $\mathbf{u_R}(z)$ is the velocity associated with the circulation. Since this model is setup for application in the context of either a single column model or sub-grid, $\nabla \cdot (\mathbf{u_b}\lambda)$ is assumed to be either 0 or handled primarily by the host model, which leaves the change in a species λ induced by the circulation as

$$\delta_t \lambda = \nabla \cdot (\mathbf{u_R}\lambda) \tag{3}$$

It is necessary to determine an appropriate model for this velocity. We assume that this velocity must depend largely on the variables associated with vertical convection that generate the circulations, namely temperature and gravity. In terms of the temperature dependence, vertical convection alone would not generate the circulations under consideration; spatial variation in the surface heating and the associated horizontal air temperature variations are necessary. Therefore, a relevant temperature scale could be the magnitude of the horizontal temperature variation of the air. As discussed previously, results in the literature also show a relationship between the size of the hot and cold patches and the magnitude of circulations, so we should expect a dependency on some length scale of heterogeneity ℓ discussed in the previous section. If we assume the flow direction to be from the low sensible heat region to the high sensible heat region, then with dimensional analysis we yield the following for u_R, the magnitude of the vector $\mathbf{u_R}$,

$$u_R(z) \sim g^{1/2} \ell^{1/2} \left(\frac{\delta \left| \theta_v'(z) \right|}{\theta_0} \right) \tag{4}$$

where $\frac{\delta \left| \theta_v'(z) \right|}{\theta_0}$ is the normalized difference in virtual potential temperature, and g is gravity. θ_0 is a normalization factor which we set to $300K$ to match a similar factor found in our single column model. This satisfies the expectation that the circulations will vanish if surface temperature is uniform ($\delta \left| \theta_v'(z) \right| = 0$) or if the size of the surface patches is sufficiently small ($\ell \to 0$) and has a functional form quite similar to a circulation speed model found in the context of analogous sea-breeze circulation literature (Miller et al., 2003).

One expectation in the literature, however, that is not satisfied is the observed phenomenon of background winds parallel to the circulation velocity reducing or outright eliminating the circulation. We take the simple proposal from Lee et al. (2019) to apply the background wind as a straight, 1:1 reduction to the original modified velocity. Adding an empirical parameter c_{ur}, we arrive at the following,

$$u_{R0} = c_{ur} g^{1/2} \ell^{1/2} \left(\frac{\delta \left| \theta_v'(z) \right|}{\theta_0} \right) \tag{5}$$

$$u_R = \begin{cases} u_{R0} - \left| u_{b\|} \right| & u_{R0} > \left| u_{b\|} \right| \\ 0 & u_{R0} \leq \left| u_{b\|} \right| \end{cases} \tag{6}$$

where $\left| u_{b\|} \right|$ is the absolute value of the component of the background wind parallel to the circulation velocity. u_R is presumed to act normal to the boundary between the hot and cold patches in the model. Notably, we only apply this equation to the circulation velocity for the lower portion of the circulation and not for the upper portion, or recirculation. This allows us to define the recirculation in a way that preserves the overall mass of the system. This circulation velocity is then used to advect heat and moisture, causing changes at each level of the circulation. Taking the primary component of interest from equation (2) and making approximations for the gradients, we get

$$\frac{d\theta}{dt}(z) = u_R(z) \frac{\Delta\theta(z)}{L} \tag{7}$$

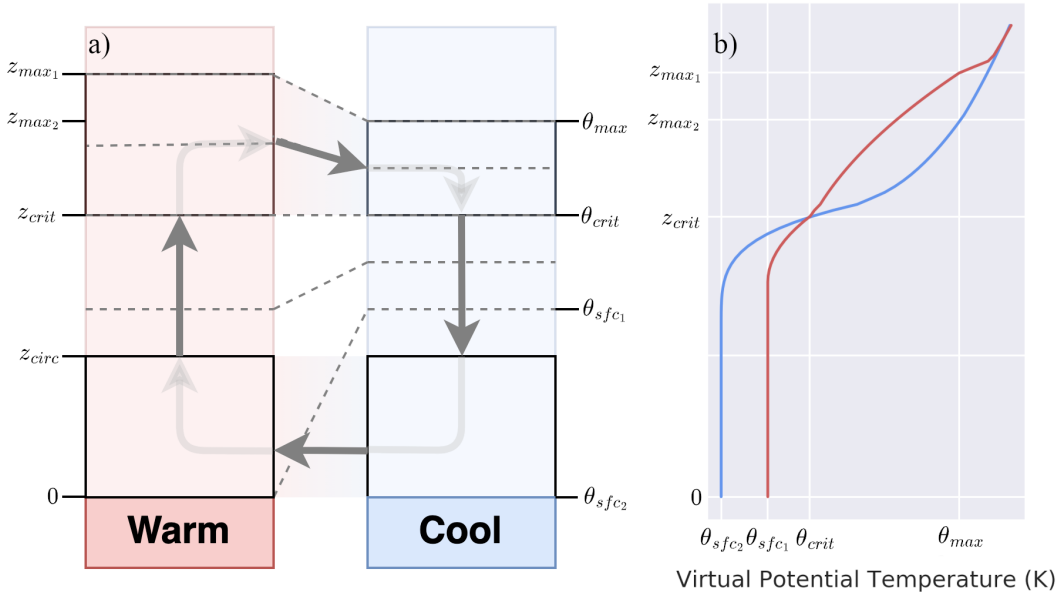

Figure 1. **a**(left): Conceptual diagram of the parameterized circulation between two columns with key virtual potential temperature limits listed. θ_{vmax}: maximum virtual potential temperature of circulation. θ_{vcrit}: minimum virtual potential temperature of the recirculation; occurs at the same height in both columns. $\theta_{v(w/c)sfc}$: virtual potential temperature at the surface of the warm and cool columns. Dashed lines indicate virtual potential temperature isotherms and solid black lines indicate boundaries of horizontal circulation. **b**(right): Illustration of idealized virtual potential temperature profiles for two columns, with key virtual potential temperature limits in **a** shown.

and

$$\frac{dq}{dt}(z) = u_R(z)\frac{\Delta q(z)}{L} \tag{8}$$

where $\frac{\Delta\theta}{L}$ and $\frac{\Delta q}{L}(z)$ are approximations for the horizontal gradients of temperature and moisture. L is an advective lengthscale between the two columns, defined in detail in the following section, and $\Delta\theta$ and Δq are the differences in temperature and moisture respectively between the two columns.

2.2 Circulation Structure and Recirculation

The structure of the circulation, the recirculation velocity, and the vertical velocities are modeled around a few bounding density values, illustrated in figure 1. From the surface to some height z_{circ} over the warm column, the horizontal flow between the two columns is defined by equation (6) and the vertical flow within the column is defined by a simple mass conservation with the incoming horizontal flow. From z_{circ} to the height of θ_{crit}, z_{crit}, there is no flow between columns and the vertical downdraft and updraft velocities of the circulation in each column are constant. Over the virtual potential temperature range of θ_{crit} to θ_{max_1}, the vertical velocity decays at a constant rate to zero. Over this same range in the cool column, the recirculation velocity is constant with height. Both the recirculation velocity and the downdraft velocity are determined, again, by a mass conservation with the velocity in the warm column in the same range.

The key bounding values are defined as follows. z_{crit} is the height at which the density of the two columns are equal, above which the warm column is more dense than the cool and below which the cool column is more dense than the warm. Above z_{crit} the density gradient implies flow from the warm to cool column, and below it the density gradient implies flow from the cool to warm column. θ_{max} represents how deeply the updraft portion of the circulation penetrates into and above the boundary layer. We expect that this level of penetration would vary based on the conditions of the simulation, and it would be computationally expensive to compute directly using an energy balance on each time step. As such, we propose the following model for θ_{max_1}:

$$\theta_{max_1} = \theta_{sfc_1} + c_1 2\sigma_{LST} \tag{9}$$

where σ_{LST} is the standard deviation of the land surface temperature and c_1 is some empirical parameter. In the limit of two grid cells or two patches, $2\sigma_{LST} = |\Delta LST|$ where $|\Delta LST|$ is the difference in land surface temperature between the two elements. This equation implies that as a parcel of air moves from column to column near the surface, it gains an energy proportional to the distance it moved along the surface temperature gradient and then rises until it has expended that energy pushing against the atmospheric virtual potential temperature gradient. The heights z_{max_1} and z_{max_2} are the heights of $\theta_{v,max}$ in the warm and cool column respectively. z_{circ} is then defined as the minimum of z_{crit} and twice $z_{max,w} - z_{crit}$. The maximum boundary of the circulation is defined this way, as opposed to simply z_{crit}, to avoid unrealistically large recirculation velocities which can occur if the lower portion of the circulation covers a depth much greater than the recirculation. In addition to being unrealistic, these large velocities can trigger numerical problems in the host single column model.

3 Methodology

3.1 Surface Fields and Parameters

The two atmospheric columns of interest for this problem are assumed to form over the regions with the highest and lowest sensible heating within the domain. We define these columns, as well as other surface characteristics of the model, from higher resolution Land Surface Model (LSM) output. For this particular study, the LSM that we use is HydroBlocks LSM, a Noah-MP based field-scale resolving land surface model (Chaney et al., 2021). The model includes high resolution soil and land cover maps from the Probabilistic Remapping of SSURGO (POLARIS) (Chaney et al., 2019) and the National Land Cover Dataset as well as NLDAS-2 meteorology (Cosgrove et al., 2003) with NCEP Stage-IV radar rainfall (Mitchell, 2004). The 30m resolution LSM is spun up for two years, and then the hourly output is modified for consistency so that the domain-wide averages match the surface fluxes that are used in the forcing data for LES and single column model runs. The forcing data is discussed in greater detail in following sections.

For application of the surface sensible and latent heat fluxes in the two column model we first upscale the field results to 5km spatial resolution. This is done to ensure that each grid cell in the domain is of sufficient scale to have atmospheric impact, as previous studies suggest (see point **(ii)** in the introduction) that smaller areas may not be large enough to generate significant circulations that penetrate through the full boundary layer. The domain is then divided into warm and cool patches based on the surface conditions for one timestep during the day (in our case, we use the surface fields at 1pm) using a cutoff value, where all grid cells or tiles with sensible heating below this value are assigned to the cool patch and all values above it are assigned to the warm patch. This cutoff value is chosen to provide the maximum difference between the patch averaged sensible heating within the bounds of the 50th and 80th percentile of domain sensible heating. The exact values of these bounds are somewhat arbitrary, however they are selected to enforce a larger cool patch than warm patch. This produces a few desirable characteristics in the circulation model, including matching expectations of a smaller portion of the

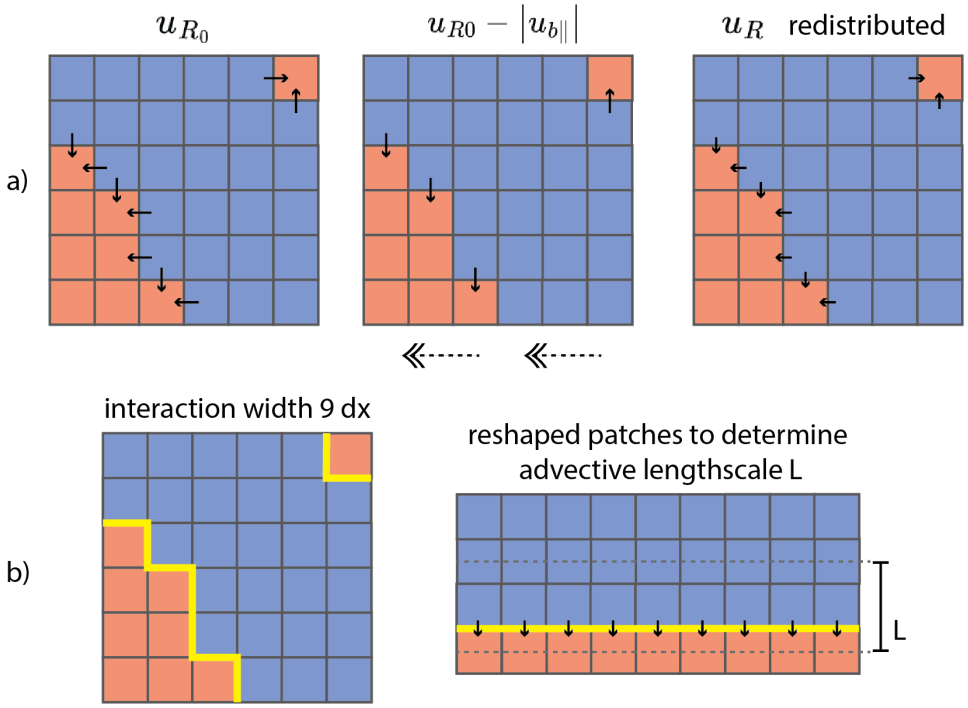

Figure 2. **a**(top): Illustration of how a background wind adjusts the velocity computed in equation (5) on an example surface grid. First panel (Left to Right) shows u_{R0}, the second shows the east-west component of u_{R0} wiped out by a strong east-west background wind, and the final one shows the final value of u_R, which is the remaining components from the second panel redistributed across the entire connecting width. **b**(bottom): Illustration of the determination of an advective lengthscale. Left panel shows the surface grid with a yellow line indicating the 9 unit boundary between the cool and warm areas. The right panel shows the same 9 unit boundary, however the shape of the grid, with the same area as the left panel, is changed to produce a straight boundary. From this regularized grid, an advective lengthscale is determined.

area covered by updrafts (over the hot patch) than downdrafts (over the cool patch), as well as encouraging larger updraft velocities than downdraft velocities (Ansmann et al., 2010).

While this separation allows for updraft and downdraft regions of the domain to exist, it does not appropriately include information on the size of the patches in the full resolution surface field, which previous studies have shown to be significant. To include patch size information in our model, we calculate a lengthscale of heterogeneity, ℓ, from the higher resolution field. This lengthscale is a measurement of how far from any given point in the field do we need to go before the correlation between the two points decays significantly. The method used is described in greater detail in (Torres-Rojas et al., 2022), with the decay cutoff in our case as 5% of the variance. This particular cutoff is chosen to produce a wide range of values for different surfaces without saturating at either end of the range. For a total of 92 surfaces of 5km resolution summer LSM output over our study domain, the values for ℓ ranged from 20km to 60km.

Surface characteristics that also need to be applied in the two column model are the geometry of the two patches and their connections; this will determine the advective lengthscale and our treatment of the background wind relative to the circulation in equation (6). Figure 2 illustrates how we consider this geometry. The circulation velocity u_R is assumed to apply over the entire interface between each column. Equation (6) is evaluated independently for the portion of the boundary along the x direction and those along the y direction, and then the final u_R used in the model is a weighted average based on the portion of the boundary along the x and y directions. The two irregularly shaped patches are reshaped to form two rectangles with the boundary length held constant. With two rectangular areas, an advective lengthscale is determined as the distance between their centroids (figure 2b).

3.2 Domain Description and Forcings

As part of this study, we examine output of a two column model, single column model, and LES over three days. These simulations and analysis of their output includes many commonalities which are discussed here. All analyses are made on a $100 \times 100\ km^2$ domain over the SGP site, centered at 36.6° N and 97.5° W. The domain consists of a few small urban areas within cultivated cropland and grasslands. The simulations use the VARANAL large-scale forcing datasets provided by the LES ARM Symbiotic Simulation and Observation Workflow (LASSO) workflow to define initial soundings and the large scale atmospheric forcings and tendencies, with the exception of large scale wind which is allowed to develop naturally from the initial sounding in LES. A tendency in the horizontal wind fields is applied for the single column and two column model simulations to nudge the large scale wind fields to match those from LES. All types of simulations run from 7:00 to 22:00 Central Daylight Time for three days: June 25th 2016, July 17th 2017, and July 9th 2018. These days are selected for initial examination due to strong heterogeneity on the surface, shallow convective conditions under which we expect significant atmospheric impacts, and clear, consistent circulations present in the LES. Figure 3 shows the surface and atmospheric conditions for select times in the LES.

3.3 Large Eddy Simulation

The LES runs that we use as our base for both parameter fitting and model comparison use a modified WRF-LES following the methodology and configuration in J. S. Simon et al. (2021) with a few differences. In these cases, we use a 250m resolution grid with a 130km x 130km simulation domain, where the surface boundary conditions from HydroBlocks LSM are tapered on the outer 15km of the domain to reduce discontinuities. This is a one way coupling and there is no feedback from the LES onto the surface. The vertical resolution is 30m for the first 5km, and then operates on a stretched

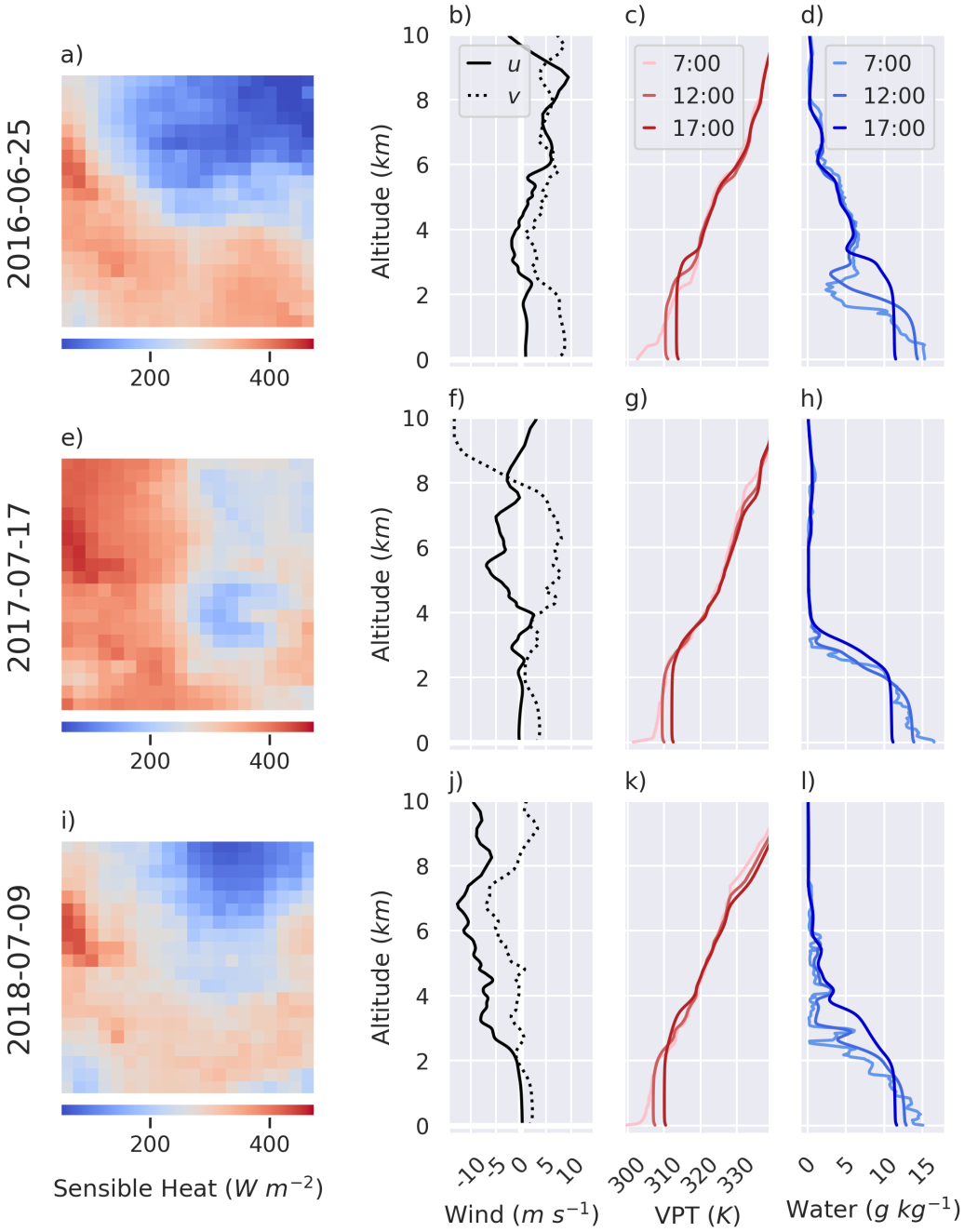

Figure 3. Surface and atmospheric profiles from LES for each day. Each row is one day, from top, June 25th, 2016, July 17th, 2017, and July 9th 2018 . **a,e,i**: 5km upscaled surface sensible heat flux for each day at 12pm. **b,f,j**: Velocity sounding at 12pm; east-west velocity as a solid line and north-south velocity as a dotted lone. **c,g,k**: Virtual potential temperature profiles at 7am, 12pm and 5pm. **d,h,l**: Atmospheric water vapor concentration profiles at 7am, 12pm and 5pm.

grid to 12km. Temporal resolution is half a second. The data used for analysis is only from the center 100km x 100km of the domain. The domain is also rotated to align the bulk liquid water flux normal to the boundaries. The model is run with periodic boundary conditions in two cases for each simulation day. The first includes the high resolution heterogeneous LSM output, which we refer to as HET, and the second includes a homogeneous surface field using the mean value of the HET surface, which we refer to as HMG. Further details of the LES configuration can be found in J. S. Simon et al. (2021).

3.4 Atmospheric Model

To apply the model described in section 2, we use a standalone simulation setup of the Cloud Layers Unified by Binormals (CLUBB) model, a cloud and turbulence parameterization scheme currently in use as part of the CESM and E3SM earth system models (Ma et al., 2022; Bogenschutz et al., 2012). The standalone version uses a simple single column model shell around CLUBB, and is run with the Morrison microphysics scheme (Morrison et al., 2005) as well as a simple radiation scheme. The model runs at a 6 second temporal resolution, and a 60m vertical resolution up to 12km. To successfully compare the model described in section 2 to a baseline as well as LES runs, we run CLUBB in three different configurations. To mimic the homogeneous LES case, and provide a baseline for model comparison, we run the standalone CLUBB as a single column with surface boundary conditions prescribed by the domain wide means. These are referred to as SC, or Single Column, simulations. We then run standalone CLUBB simultaneously over two independent columns, with surface boundary conditions prescribed by the warm and cool patch mean values determined following the methodology in section 3.1. These are referred to as IC, or Independent Columns, simulations. Finally, we run standalone CLUBB simultaneously over two independent columns, as in the IC case, but with the circulation model described implemented. We refer to this as the TCM, or two-column model, case.

For the TCM case, only heat and moisture are advected between the two columns whereas within the columns a mean vertical velocity is prescribed to match the updraft and downdraft velocities from the circulation model. The heat and moisture advection is added as a source term at each level in the model. The circulation terms are calculated every 5 minutes during the day, and only begins when there is a minimum of 300 $W\ m^{-2}$ incoming shortwave radiation. To promote model stability, change in u_R from one timestep to the next is limited to a maximum of 0.5 $m\ s^{-1}$. In addition, before the profile of computed u_R values according to equation (6) are applied to the standalone columns, a beta function is used to smooth the profile. This is done to prevent sharp vertical gradients in the resulting source terms at the edges of the circulation and recirculation.

3.5 Parameter Fitting

For these initial experiments, we conduct a relatively simple parameter fitting to the LES data. The value of c_1, held as the same for all three study days, is selected visually based on the full set of 92 LES simulation days, and c_{ur} is fitted individually for each day with LES data. To fit either of these parameters, we must have an approximation for the one-dimensional velocity of the circulation from the LES. We are largely looking to examine large (km) scale phenomenon, so a Gaussian filter is applied to the velocity fields before examining them to reduce the impact of small scale events. For a first order approximation, we take the following for each layer:

$$\max\left(\left|u_{90_i}\right|, \left|u_{10_i}\right|\right) = u_{R0*} \tag{10}$$

where $i = 1, 2$, and u_{90_i} is the 90th percentile of the smoothed horizontal velocity in the i direction, u_{10_i} is the 10th percentile, and u_{R0*} is the approximate value of u_{R0} computed from the LES. We take each percentile as we assume that the circulation will cause

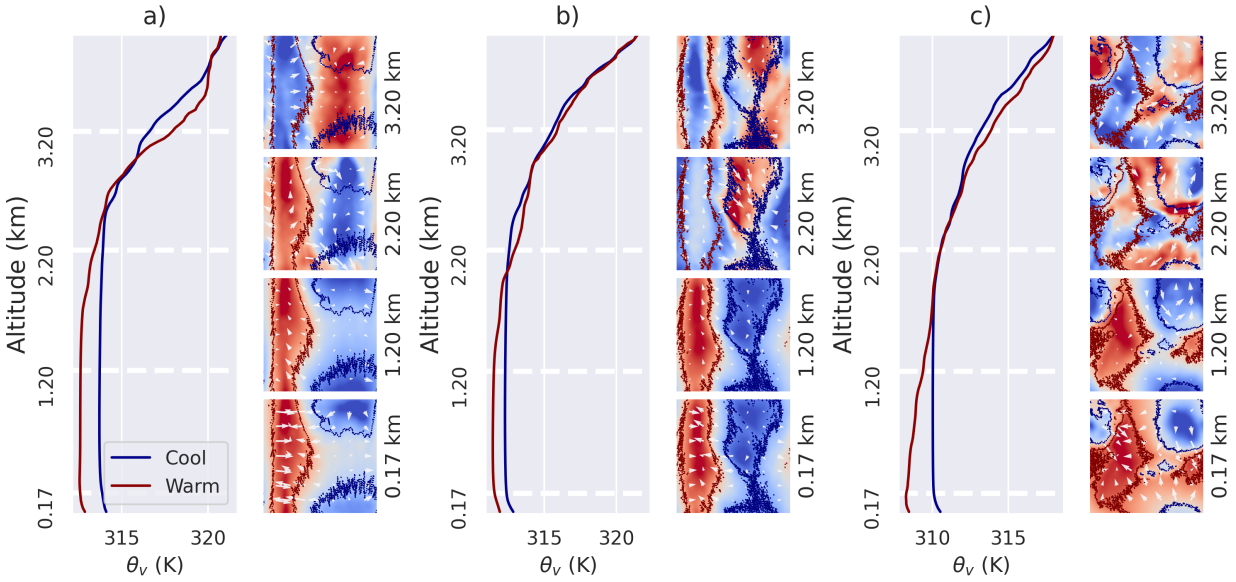

Figure 4. Vertical LES profile at 5pm of a "cool" and "warm" patch defined based on the 25th and 75th percentiles respectively of virtual potential temperature at 150m for each day: 2016-06-25 (a), 2017-07-17 (b), and 2018-07-09 (c). The horizontal field of virtual potential temperature is shown to the right of these profiles for four altitudes: 170m, 1200m, 2200m and 3200m. The arrows represent the horizontal velocity deviations $u\prime$. The contour lines show the bounding areas of the "cool" and "warm" patches whose profiles are plotted directly to the left.

two opposing velocities converging on the hot region, which is a reasonable assumption given the periodic boundary conditions in the LES. We also assume that, by taking the larger magnitude of these two percentiles, we are capturing the mean enhanced wind (i.e. $u_r + |u_{w\|}|$) which allows us to rearrange equation (6) to get equation (10). If u_{90_i} and u_{10_i} have the same sign, then it is assumed no circulation is occurring in that direction. While the heterogeneity may well be inducing circulations, they are carried too quickly by background winds to be represented well by our model.

In addition to requiring circulation velocities, we also need to identify two "columns" within the LES to generate adequate comparisons. While we identify these based on the surface for the two-column model, in the LES we found that the representative columns are better defined from the near surface atmospheric virtual potential temperature. We therefore divide the domain into two columns, constant in height, based on the method described in section 3.1 using the 150m virtual potential temperature layer instead of the sensible heat flux to divide them.

The fit exercise is conducted for a total of 92 simulation days, of which 43 had a detectable circulation fitting the criteria described. Three of those simulation days had coherent front-like systems which crossed the domain, making the results unreliable for fitting with (10) and were therefore excluded, bringing the total number of LES simulation days used for our fitting exercise to 40.

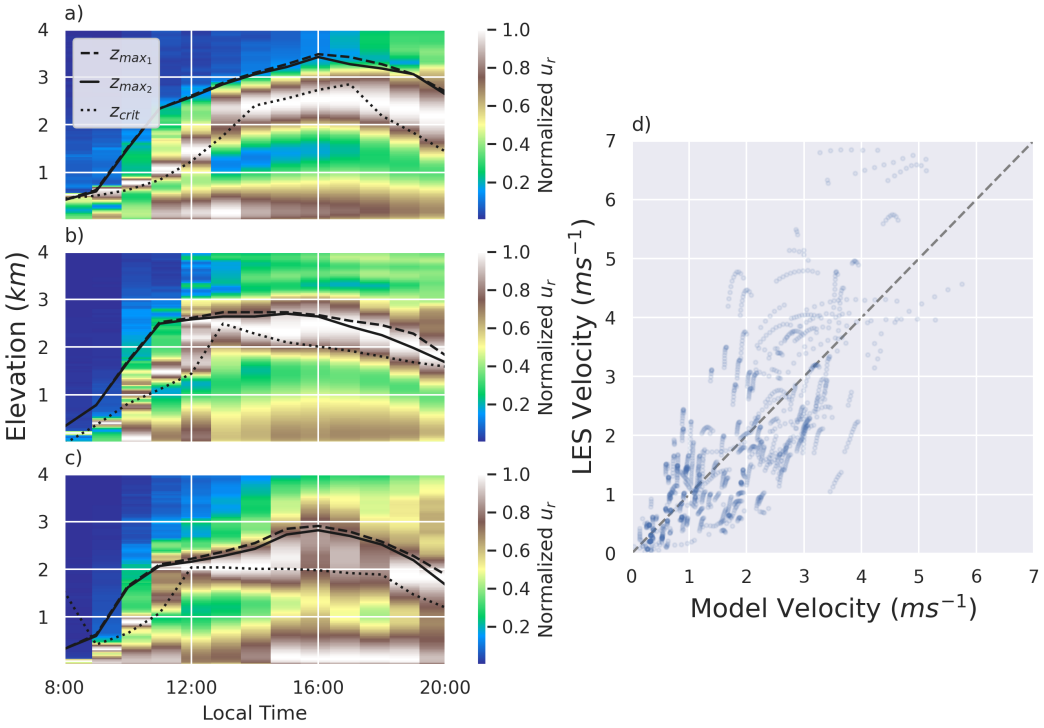

Figure 5. **a,b,c**: Profile of normalized circulation velocity through time, with velocity computed as in equation (10) for each day: 2016-06-25 (a), 2017-07-17 (b), and 2018-07-09 (c). No points were excluded based on differences in sign from u_{90_i} and u_{10_i}. Lines plotted are z_{max_1} (dashed), z_{max_2} (solid), and z_{crit} (dotted) showing the bounds of the recirculation defined in section 2.2. **d**: Comparison between the modeled circulation velocity with $c_1 = 1.35$ and the LES computed circulation velocity during the day (10:00-19:00) for the first 500m in the atmosphere over 40 LES simulation days.

4 Results

4.1 Characteristics of Modeled Circulation

First, we must ensure that the general model, described in previous sections, is consistent with what we see in the large eddy simulations. We are consistently able to see the behavior illustrated in figure 1 for the θ_v profiles across nearly all LES days, with an intersection point at some altitude where the density gradient flips. Figure 4 shows vertical profiles for identified "cool" and "warm" areas based on the 25th and 75th percentile of virtual potential temperature at 150m, as well as wind velocities $u\prime$. When examining the lowest shown surface for each level on the three days, there is a clear convergence over the warm areas and divergence from the cool areas. In the upper portion of the atmosphere, where the density gradient reverses and the "cool" patch becomes warmer than the "warm" patch, there is instead a noticeable divergence from the 150m-based "warm" patch. This lends significant credence to the validity of the basic structure we propose for TCM.

These two columns also appear to be consistent with the boundaries that were defined in section 2.2. Using those definitions with the LES defined columns, we see fairly successful bounding of the region of highest circulation velocity in the LES profile as is clear from figure 5abc. For the upper boundaries of the recirculation, there is a good agree-

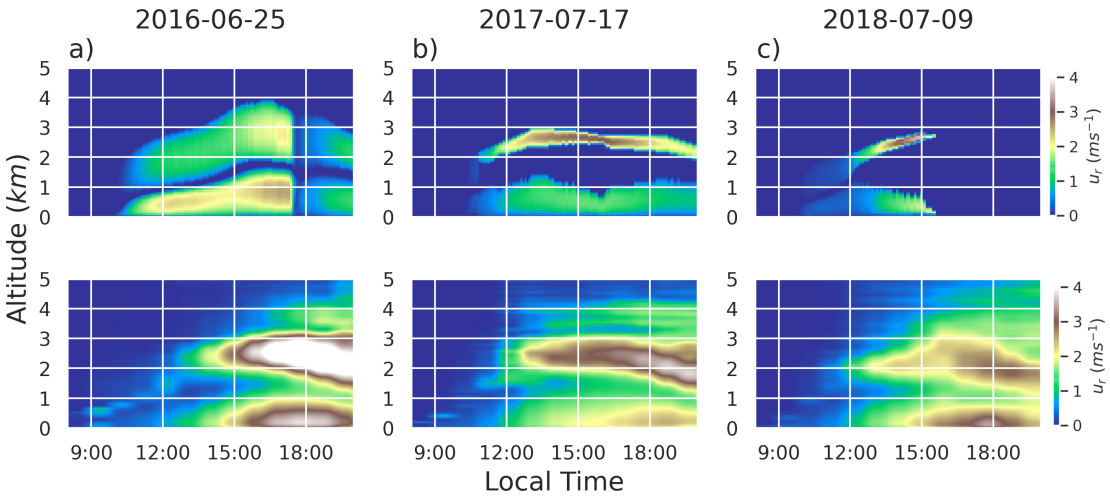

Figure 6. Circulation velocity profile through time for TCM (top) and LES (bottom) for each day 2016-06-25 (a), 2017-07-17 (b), and 2018-07-09 (c).

ment for all three days with a small underprediction for some times on 2017-07-17 and 2018-07-09 and a small overprediction on 2016-06-25. The identification of z_{crit} as the lower bounds of the recirculation, however, does not perform as well with a consistent overprediction of the value ranging from 100m to nearly 800m depending on the day and time. When we examine the proposed velocity model (6) we also see a reasonable fit as seen in figure 5d. When the model predicted velocity from the temperature fields is compared to the true LES field, we get a R^2 value of 0.56 and a fitted c_1 value of 1.35.

When the circulation model is fully implemented in the two column model, we see a stable circulation develop as is clear in the top row of figure 6. The circulations largely lie between 2 and 3km in the atmosphere during the afternoon, with horizontal velocities in a reasonable range from 0 to 3.5 $m\ s^{-1}$ and vertical velocities of up to $0.25m\ s^{-1}$. Circulations initiate around 10:30 am for all three days. While the 2016 and 2017 days maintain a circulation throughout the day, the 2018 circulation thins in the afternoon until it disappears shortly after 3pm when the computed value of θ_{max} is at or below θ_{crit}, preventing continued simulation. A slowdown event can also be observed on 2016-06-25 in the early evening; this occurs because the circulation preceding the slowdown was strong enough to bring the temperature of the cool and warm atmospheric columns to near equilibrium, significantly lowering the value of $\delta\,|\theta_v'|$ and u_R accordingly.

When compared with the LES days, we see some broad similarities in velocity profiles, but with significant differences. Direct comparison of the altitude in the profile is somewhat complicated by the three dimensional nature of the LES, where the altitude of the circulation could vary significantly in space compared to the one-dimensional TCM. Nonetheless, LES profiles are similarly located primarily between 2 and 3km in altitude, although with a more significant decay in altitude during the later portion of the day than TCM. The LES and TCM circulations have relatively similar thicknesses, although the same cannot be said of the recirculation which is thicker on 2016-06-25, thinner on 2017-07-17, and much thinner on 2018-07-09. Velocities are mostly larger in the LES than in TCM, although the recirculation velocity on 2017-07-17 is practically the same between 12:00 and 5:00pm. The circulation is also very similar between 12:00 and 3:00pm

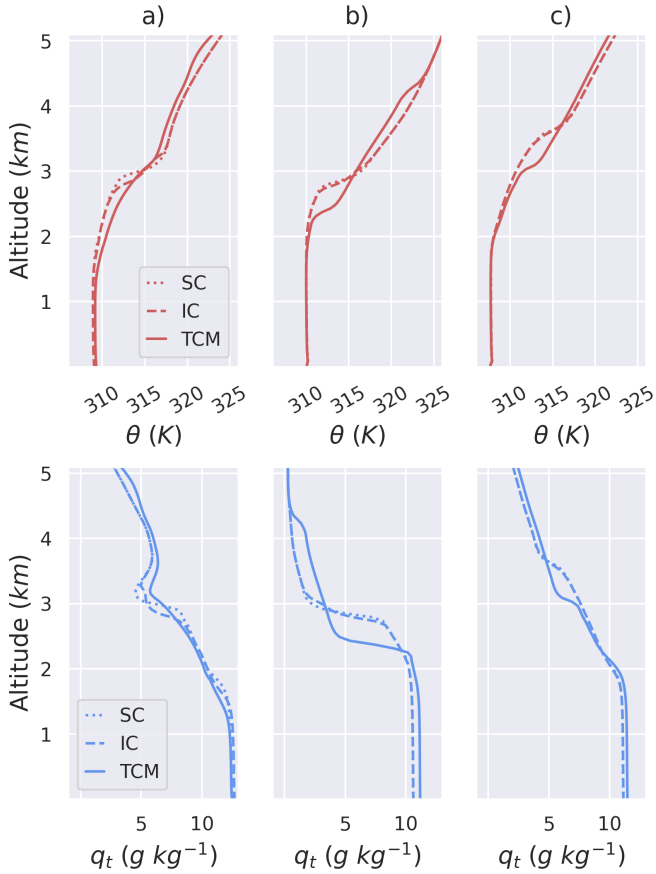

Figure 7. Profiles at 5pm of temperature (top) and moisture (bottom) for the first 5km of all three CLUBB based cases SC, IC, and TCM; dotted, dashed and solid lines respectively. Columns are days 2016-06-25 (a), 2017-07-17 (b), and 2018-07-09 (c).

for 2018-08-09. For 2016-06-25, the circulation velocity is off by almost $1ms^{-1}$ and the recirculation is off more significantly.

4.2 Atmospheric Impacts of the Circulation

Heterogeneity-driven circulations have significant impacts on the atmosphere in both the LES and TCM. The impacts are visible in the profiles of heat and moisture and in the clouds that are produced in the model. While differences exist between LES and TCM, they both exhibit qualitatively similar behaviors with regards to their impact on the atmosphere.

The profiles of temperature and moisture provide the first clue to the atmospheric impacts of the circulations. Under the IC case, there are only small differences when compared to SC; mostly just a very small reduction in the depth of the boundary layer on both 2016-06-25 and 2017-07-17, which is also visible in the profiles for moisture. When the circulation is added, the TCM case shows consistent heating near the top of the boundary layer and a cooling above it in figure 7. A similar, albeit less dramatic, change is observed in the LES profiles in figure 8. The LES profiles of temperature bear a very strong similarity to the TCM profiles for all three days (except with a smoother curve as would be expected from the 100km domain spatial averaging).

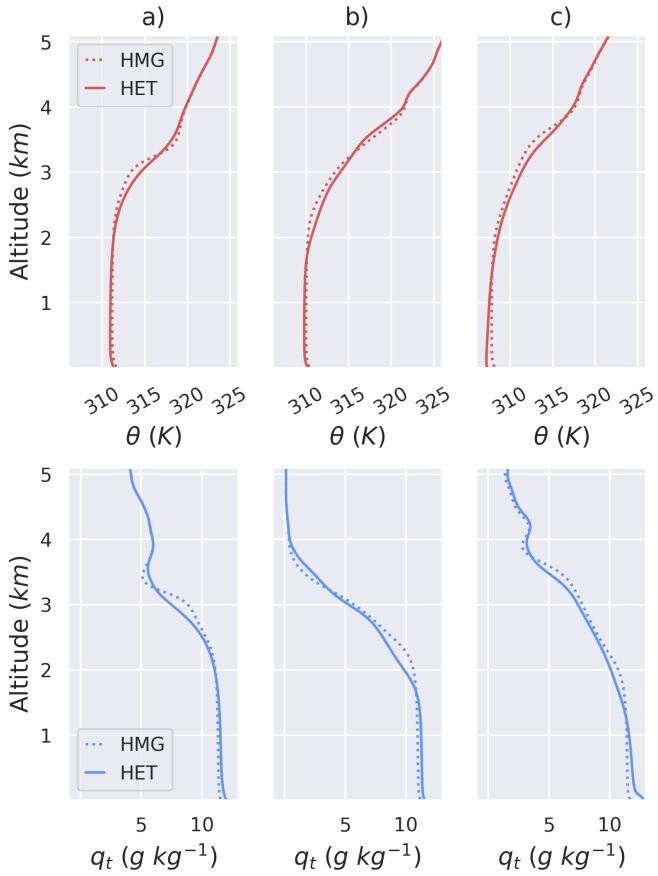

Figure 8. Profiles at 5pm of temperature (top) and moisture (bottom) for the first 5km of both of the LES based cases HMG and HET; dotted and solid lines respectively. Columns are days 2016-06-25 (a), 2017-07-17 (b), and 2018-07-09 (c).

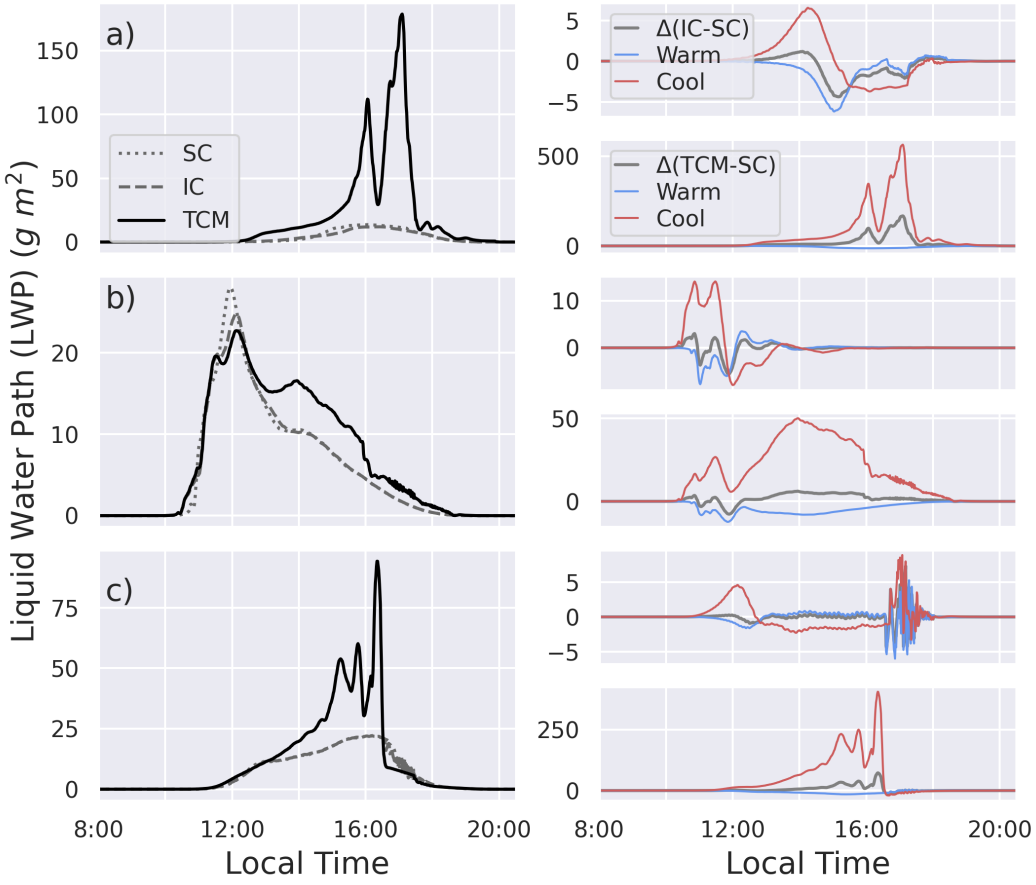

Figure 9. The liquid water path (LWP) output from the CLUBB based cases, with rows as days 2016-06-25 (a), 2017-07-17 (b), and 2018-07-09 (c). LWP through time is shown for each of the three cases (left of each row). Difference in LWP between the IC case and SC case as well as difference between the warm and cool columns of the IC case and the SC case (upper left of each row). Difference in LWP between the TCM case and SC case as well as difference between the warm and cool columns of the TCM case and the SC case are also shown.

Some consistent patterns of change occur in the mean moisture profile as well. When heterogeneity is added without a modeled circulation in the IC case, there are very few changes from SC. When the modeled circulation is added, there is a slight overall wetting near the surface on 2017-07-17 and 2018-07-09, a drying around the top of the boundary layer that coincides with the location of the circulation and then a wetting of the atmosphere above. On 2016-06-25 there is no near surface wetting and instead a near surface drying; in addition, the changes higher in the atmosphere are less pronounced. The LES sees largely the same trends, but smoothed as its averaged over the whole domain, and a lower magnitude in differences. While we don't see the drying of the boundary layer on 2016-06-25 in the LES, it does have the least significant wetting of the three days examined.

All of these changes in the scalar profiles are closely related to the changes that we see in cloud development as a result of the TCM. The liquid water path (LWP) is a proxy for cloud development, and is defined as:

$$\Sigma \rho_a q_l \Delta_z \tag{11}$$

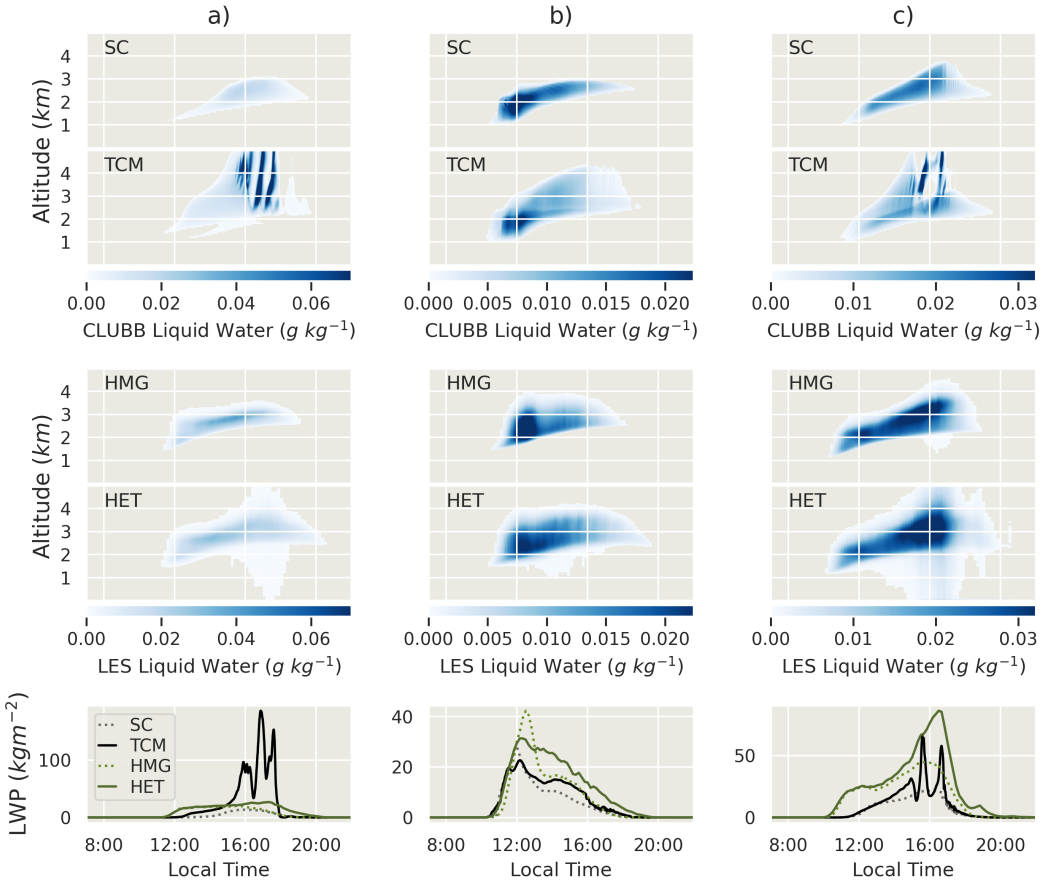

Figure 10. Comparison of cloud structure through time for the SC, TCM, HMG, and HET simulations for each day (columns) 2016-06-25 (a), 2017-07-17 (b), and 2018-07-09 (c). Cloud liquid water concentration shown for the CLUBB based simulations, SC (top) and TCM (second from top) followed by the two LES based cases, HMG (third from top) and HET (fourth from top). Finally, LWP through time is shown for these four cases (bottom).

where ρ_a is the moist air density, q_l is the liquid water mixing ratio, and z is the vertical. LWP increases under the TCM case. The IC case produces some small changes on each day, but largely fails to create significant differences. The circulation, however, yields increases in LWP especially later in the day as seen in figure 9. The LWP increases collapse when the circulation does, as is clear on 2018-07-09. In TCM we also see the concentration of cloud development over the warm column rather than the cool in right side of figure 9. This pattern is not clearly visible in the IC case without a circulation, but is regularly observed in LES studies. The LWP in the cool columns of the TCM case is also depressed, mimicking another finding in the literature. Two of the days show significant spikes in LWP and are not as smooth on the TCM as the SC and IC days. This may be caused by some small numerical issues in CLUBB when the hole filling scheme, which corrects for situations where the CLUBB solver predicts negative concentrations, is forced to activate that we were unable to completely resolve. Varying the spatial and temporal resolutions of the model did change the frequency of hole scheme activation, however yielded little changes in the overall pattern of cloud and LWP development.

The vertical profiles of cloud liquid water in figure 10 show the changes in vertical structure that are caused by including heterogeneity driven circulations in both LES (moving from HMG to HET) and the CLUBB-based setup (from SC to TCM). In both the HET and TCM cases, we see an increase in the depth of the cloud, although this is more pronounced in the TCM case. It is notable, however, that the cloud starts significantly thinner in all three of the SC cases compared to the HMG cases. The cloud LWP changes are quite similar between HET and TCM for 2017-07-17 and 2018-07-09 in both timing and magnitude, whereas on 2016-06-25 we see a huge LWP increase in the TCM case but only a small LWP increase in the HET case. The higher depth of the circulation for that day in TCM when compared to HET may explain these differences.

5 Discussion

5.1 Comparisons with LES and their Limitations

From a broad perspective, the two-column model is able to produce circulations with key characteristics identified in the literature from LES studies, including flow velocity that scales with surface heterogeneity, sensitivity to background wind conditions, enhancement of cloud formation that is concentrated over the warmer regions, and reasonable horizontal breeze velocities. Closer examination of this model in an LES framework, as well as comparing these LES results quantitatively to TCM, poses some limitations that must be discussed. First, it should be noted that the results from the SC case and the HMG case, while close, do not match. While steps were taken to bring the SC case closer to the HMG case, we were ultimately unable to achieve perfect agreement in this simplest case, which also means that the addition of heterogeneity to both models is not as directly comparable. While profiles analogous to the two columns can be identified within LES, these 'columns' are not independent. Non-circulatory advection, turbulent diffusion, etc. are constantly occurring between the columns, providing a major source of disagreement between the TCM and HET cases, even when assuming a perfect representation of the advection caused by heterogeneity driven circulations. The impact of non-circulatory advection is most important when examining the periodic boundary conditions, which allow for the enhancement or suppression of surface heterogeneities in the atmosphere when compared to TCM. A particularly potent example of this is the 2016-06-25 day. On this day, a strong background wind to the north causes the patterns of heterogneity at the surface (figure 3a) to shear and blend into alternative patterns in the lower atmosphere (figure 4). The periodic boundary conditions allow for warm air to be continuously pushed over the warm patch, and the cool air over the cool patch, ramping up and increasing the differences in temperature beyond what is likely in the environment. This "ramping up" would not be captured in TCM with the external forcing used and the lack of advection, causing a significant difference in the atmospheric temperature gradients experienced in each model. This difference could explain some of the large differences in velocity apparent between TCM and HET for this particular day. One final major discrepancy is the variability of the surface patch geometry through time. In LES, the organization of the heterogeneity is allowed to change through time, however in TCM the patch geometry is set for the entire day. On days with high spatiotemporal persistence this is not an issue, however on days where the patch location changes throughout the day, LES has the advantage to better model circulations.

While there is significant agreement between the model, the literature, and the data, there are some notable differences. On 2018-07-09, we see that the TCM circulation has a much smaller thickness, and decays quickly when compared to the LES in figure 6. There is a similar smaller thickness on 2017-07-17 and when we examine the model predicted boundaries in figure 5. For all three days, the lower recirculation boundary, z_{crit} is higher than the lower bound we would define based on the velocity profiles. (Rochetin et al., 2017) finds in their study that "Through the day, the breeze intensity and direction is successively dominated by (i) the low-level large-scale wind, (ii) the horizontal temper-

ature gradients and (iii) the overturning mesoscale circulation itself'. The first two points are adequately considered in the proposed model, however the self-sustaining ability of the circulation is not considered which may explain some of these described problems. If properly considered, the flow would likely maintain later on 2018-07-09 and the depth of the recirculation may extend slightly below z_{crit} as the flow is allowed to influence adjacent areas just outside the flow regime. This could also explain the fact that the velocity appears to peak between 15:00 and 17:00 whereas in the LES it peaks at or after 18:00.

5.2 Parameter Tuning

While the original parameter tuning shows success, additional tuning could likely improve performance further. The velocity is overall lower in TCM than LES. One likely explanation is already discussed as the increased velocity due to the self-reinforcing temperature fields as a result of the periodic boundary conditions, although this doesn't explain days where this doesn't apply. Another possible explanation is the model overestimating the reduction in circulation velocity caused by the mean wind. While the model uses a 1:1 reduction as suggested in Lee et al. (2019), sea breeze literature proposes a much smaller reduction (Miller et al., 2003). The change to using the lower background wind reduction is on the order of the differences we see between HET and TCM, however to adequately assess the magnitude of reduction caused by background wind for land surface driven circulations, an additional LES study would need to be conducted. Other tuning may be helpful to solve discrepancies such as the high LWP on 2016-06-25. The high LWP is caused by a deeper penetration into the boundary layer than in the LES. The tuning exercise for c_1 in equation (9) was limited and a more in depth quantitative examination of this parameter may yield improvements on days such as 2016-06-25.

5.3 Pathways for Implementation in ESMs

The two-column structure has potential for application in ESMs. Additional computational costs of adding an additional single column model within the ESM grid cell are significant, but the additional costs from the circulation model itself should be rather small if correctly optimized. It is notable that the model code as applied for this study is admittedly sub-optimal, using a python script to interface with the CLUBB FORTRAN code and requires excessive I/O operations that would be unnecessary in optimized code. While in this particular study a regular grid is used for the surface, the methodology lends itself to using aggregation of tiles from tiling schemes to determine surface columns rather than aggregation of grid cells. The identification of those surface columns, however, is not as clear in the coupled modeling context where surface heterogeneity will not be known a priori. In our study area of the Southern Great Plains, the heterogeneity is largely driven by rainfall patterns the previous day. An assumption of some environmental characteristics driving the pattern of heterogeneity, such as rainfall patterns, or an assumption of high spatiotemporal persistence (i.e. that the previous afternoons' patterns of heterogeneity will persist into the next day) would be necessary for proper aggregation of the surface tiles. We note that some LSMs may face additional development needs if no representation of subgrid-scale precipitation exists currently, and/or if there is no spatial representation of surface heterogeneity (i.e., surface tiles are allocated statistically).

Although one pathway towards implementation within ESMs is to directly simulate two atmospheric columns and link them via a circulation as described here, there is also an opportunity to take advantage of existing atmospheric model development. Multiplume eddy-diffusivity mass-flux (EDMF) parameterizations simulate convective updrafts that transport heat and moisture vertically and are being implemented within schemes including CLUBB (Witte et al., 2022). As ongoing development works to include explicit downdrafts in EDMF schemes, it is conceivable that some number of updrafts/downdrafts could be used to represent heterogeneity-induced circulations with the type of model pro-

posed here. One advantage of any scheme to capture heterogeneity driven circulations is that it is only expected to be significant when certain criteria can be met (high spatiotemporal persistence, significant heterogeneities, and low background wind). This means the scheme only needs to be activated when applicable, saving computational cost.

6 Summary and Conclusion

Our work shows that a simple two-column model of surface heterogeneity driven large-scale (10km) circulations can qualitatively reproduce the patterns that we see in both our own LES simulations and the larger body of literature. We see agreement both with the model structure within the LES data, as well as agreement when the model structure is applied to two otherwise independent single column CLUBB simulations. Cloud production is both increased and concentrated over the warmer surface patch when the circulations are considered, and for two of the three days these changes bear a strong similarity to LWP changes seen in the LES. Circulation strength is closely related to surface patterns, atmospheric profiles of temperature and moisture, and the direction and magnitude of the background wind as expected from the literature. There are some key differences in the details that suggest that more tuning, testing, and accounting for the self-sustaining ability of the circulations may resolve the discrepancies between HET and TCM. There is potential for the model structure described here to be implemented in coarse grid models where global, atmospheric impacts of subgrid land surface heterogeneity could be more readily explored. The similarities that land surface heterogeneity circulations have with other thermally driven circulations imply that the model may also be applicable to subgrid-scale parameterization of sea and lake breezes. This work resembles a promising step towards accounting for the increased cloud production and atmospheric impacts caused by subgrid heterogeneity driven circulations in ESMs.

7 Open Research

Software used to run the two column model in SC, IC and TCM cases is available from Zenodo (Waterman, 2023). The base WRF-LES code, initial sounding profiles and large-scale forcing files are available from (Gustafson et al., 2020). Additional modifications to the WRF-LES code to specify the varying surfaces are available from (J. Simon & Chaney, 2021).

Acknowledgments

This research has been supported by NA19OAR4310241 - Parameterizing the effects of sub-grid land heterogeneity on the atmospheric boundary layer and convection: Implications for surface climate, variability, and extremes. As well as NA220AR0AR4310644 - Implications of heterogeneity-aware land-atmosphere coupling in the predictability of precipitation extremes.

References

Ansmann, A., Fruntke, J., & Engelmann, R. (2010, August). Updraft and downdraft characterization with Doppler lidar: cloud-free versus cumuli-topped mixed layer. *Atmospheric Chemistry and Physics*, *10*(16), 7845–7858. Retrieved 2023-05-12, from `https://acp.copernicus.org/articles/10/7845/2010/` doi: 10.5194/acp-10-7845-2010

Avissar, R., & Liu, Y. (1996, March). Three-dimensional numerical study of shallow convective clouds and precipitation induced by land surface forcing. *Journal of Geophysical Research: Atmospheres*, *101*(D3), 7499–7518. Retrieved 2023-05-12, from `http://doi.wiley.com/10.1029/95JD03031` doi: 10.1029/95JD03031

Avissar, R., & Schmidt, T. (1998, August). An Evaluation of the Scale at which Ground-Surface Heat Flux Patchiness Affects the Convective Boundary Layer Using Large-Eddy Simulations. *Journal of the Atmospheric Sciences*, *55*(16), 2666–2689. Retrieved 2023-04-28, from http://journals.ametsoc.org/doi/10.1175/1520-0469(1998)055<2666:AEOTSA>2.0.CO;2 doi: 10.1175/1520-0469(1998)055⟨2666:AEOTSA⟩2.0.CO;2

Bogenschutz, P. A., Gettelman, A., Morrison, H., Larson, V. E., Schanen, D. P., Meyer, N. R., & Craig, C. (2012, November). Unified parameterization of the planetary boundary layer and shallow convection with a higher-order turbulence closure in the Community Atmosphere Model: single-column experiments. *Geoscientific Model Development*, *5*(6), 1407–1423. Retrieved 2023-05-12, from https://gmd.copernicus.org/articles/5/1407/2012/ doi: 10.5194/gmd-5-1407-2012

Bonan, G. B., Oleson, K. W., Vertenstein, M., Levis, S., Zeng, X., Dai, Y., ... Yang, Z.-L. (2002, November). The Land Surface Climatology of the Community Land Model Coupled to the NCAR Community Climate Model*. *Journal of Climate*, *15*(22), 3123–3149. Retrieved 2023-05-12, from http://journals.ametsoc.org/doi/10.1175/1520-0442(2002)015<3123:TLSCOT>2.0.CO;2 doi: 10.1175/1520-0442(2002)015⟨3123:TLSCOT⟩2.0.CO;2

Chaney, N. W., Minasny, B., Herman, J. D., Nauman, T. W., Brungard, C. W., Morgan, C. L. S., ... Yimam, Y. (2019, April). POLARIS Soil Properties: 30-m Probabilistic Maps of Soil Properties Over the Contiguous United States. *Water Resources Research*, *55*(4), 2916–2938. Retrieved 2023-05-12, from https://onlinelibrary.wiley.com/doi/abs/10.1029/2018WR022797 doi: 10.1029/2018WR022797

Chaney, N. W., Roundy, J. K., Herrera-Estrada, J. E., & Wood, E. F. (2015, January). High-resolution modeling of the spatial heterogeneity of soil moisture: Applications in network design. *Water Resources Research*, *51*(1), 619–638. Retrieved 2023-05-13, from http://doi.wiley.com/10.1002/2013WR014964 doi: 10.1002/2013WR014964

Chaney, N. W., Torres-Rojas, L., Vergopolan, N., & Fisher, C. K. (2021, November). HydroBlocks v0.2: enabling a field-scale two-way coupling between the land surface and river networks in Earth system models. *Geoscientific Model Development*, *14*(11), 6813–6832. Retrieved 2023-05-13, from https://gmd.copernicus.org/articles/14/6813/2021/ doi: 10.5194/gmd-14-6813-2021

Chaney, N. W., Van Huijgevoort, M. H. J., Shevliakova, E., Malyshev, S., Milly, P. C. D., Gauthier, P. P. G., & Sulman, B. N. (2018, June). Harnessing big data to rethink land heterogeneity in Earth system models. *Hydrology and Earth System Sciences*, *22*(6), 3311–3330. Retrieved 2023-05-12, from https://hess.copernicus.org/articles/22/3311/2018/ doi: 10.5194/hess-22-3311-2018

Cosgrove, B. A., Lohmann, D., Mitchell, K. E., Houser, P. R., Wood, E. F., Schaake, J. C., ... Meng, J. (2003, November). Real-time and retrospective forcing in the North American Land Data Assimilation System (NLDAS) project. *Journal of Geophysical Research: Atmospheres*, *108*(D22), 2002JD003118. Retrieved 2023-05-12, from https://onlinelibrary.wiley.com/doi/abs/10.1029/2002JD003118 doi: 10.1029/2002JD003118

Crosman, E. T., & Horel, J. D. (2010, October). Sea and Lake Breezes: A Review of Numerical Studies. *Boundary-Layer Meteorology*, *137*(1), 1–29. Retrieved 2023-04-23, from http://link.springer.com/10.1007/s10546-010-9517-9 doi: 10.1007/s10546-010-9517-9

Ducharne, A., Koster, R. D., Suarez, M. J., Stieglitz, M., & Kumar, P. (2000, October). A catchment-based approach to modeling land surface processes in a general circulation model: 2. Parameter estimation and model demonstration.

Journal of Geophysical Research: Atmospheres, *105*(D20), 24823–24838. Retrieved 2023-05-12, from http://doi.wiley.com/10.1029/2000JD900328 doi: 10.1029/2000JD900328

Eder, F., De Roo, F., Rotenberg, E., Yakir, D., Schmid, H. P., & Mauder, M. (2015, October). Secondary circulations at a solitary forest surrounded by semi-arid shrubland and their impact on eddy-covariance measurements. *Agricultural and Forest Meteorology*, *211-212*, 115–127. Retrieved 2023-04-23, from https://linkinghub.elsevier.com/retrieve/pii/S016819231500180X doi: 10.1016/j.agrformet.2015.06.001

Garcia-Carreras, L., Parker, D. J., & Marsham, J. H. (2011, March). What is the Mechanism for the Modification of Convective Cloud Distributions by Land Surface–Induced Flows? *Journal of the Atmospheric Sciences*, *68*(3), 619–634. Retrieved 2023-04-23, from https://journals.ametsoc.org/doi/10.1175/2010JAS3604.1 doi: 10.1175/2010JAS3604.1

Golaz, J.-C., Larson, V. E., & Cotton, W. R. (2002, December). A PDF-Based Model for Boundary Layer Clouds. Part I: Method and Model Description. *Journal of the Atmospheric Sciences*, *59*(24), 3540–3551. Retrieved 2023-05-12, from http://journals.ametsoc.org/doi/10.1175/1520-0469(2002)059<3540:APBMFB>2.0.CO;2 doi: 10.1175/1520-0469(2002)059⟨3540:APBMFB⟩2.0.CO;2

Gustafson, W. I., Vogelmann, A. M., Cheng, X., Dumas, K. K., Endo, S., Johnson, K. L., ... Xiao, H. (2020, 9). Description of the lasso data bundles product. *DOE Office of Science Atmospheric Radiation Measurement (ARM) Program*. Retrieved from https://www.osti.gov/biblio/1469590 doi: 10.2172/1469590

Hadfield, M. G., Cotton, W. R., & Pielke, R. A. (1991, October). Large-eddy simulations of thermally forced circulations in the convective boundary layer. Part I: A small-scale circulation with zero wind. *Boundary-Layer Meteorology*, *57*(1-2), 79–114. Retrieved 2023-04-28, from http://link.springer.com/10.1007/BF00119714 doi: 10.1007/BF00119714

Han, C., Brdar, S., & Kollet, S. (2019, December). Response of Convective Boundary Layer and Shallow Cumulus to Soil Moisture Heterogeneity: A Large-Eddy Simulation Study. *Journal of Advances in Modeling Earth Systems*, *11*(12), 4305–4322. Retrieved 2023-04-23, from https://onlinelibrary.wiley.com/doi/abs/10.1029/2019MS001772 doi: 10.1029/2019MS001772

Huang, M., Ma, P.-L., Chaney, N. W., Hao, D., Bisht, G., Fowler, M. D., ... Leung, L. R. (2022, August). Representing surface heterogeneity in land–atmosphere coupling in E3SMv1 single-column model over ARM SGP during summertime. *Geoscientific Model Development*, *15*(16), 6371–6384. Retrieved 2023-05-14, from https://gmd.copernicus.org/articles/15/6371/2022/ doi: 10.5194/gmd-15-6371-2022

Kang, S.-L., & Bryan, G. H. (2011, September). A Large-Eddy Simulation Study of Moist Convection Initiation over Heterogeneous Surface Fluxes. *Monthly Weather Review*, *139*(9), 2901–2917. Retrieved 2023-04-28, from https://journals.ametsoc.org/doi/10.1175/MWR-D-10-05037.1 doi: 10.1175/MWR-D-10-05037.1

Kang, S.-L., & Ryu, J.-H. (2016, July). Response of moist convection to multi-scale surface flux heterogeneity: Response of Moist Convection to Multi-scale Surface Flux Heterogeneity. *Quarterly Journal of the Royal Meteorological Society*, *142*(698), 2180–2193. Retrieved 2023-04-28, from https://onlinelibrary.wiley.com/doi/10.1002/qj.2811 doi: 10.1002/qj.2811

Lee, J. M., Zhang, Y., & Klein, S. A. (2019, February). The Effect of Land Surface Heterogeneity and Background Wind on Shallow Cumulus Clouds and the Transition to Deeper Convection. *Journal of the Atmospheric Sciences*, *76*(2), 401–419. Retrieved 2023-04-23, from https://journals.ametsoc.org/doi/

10.1175/JAS-D-18-0196.1 doi: 10.1175/JAS-D-18-0196.1

Ma, P.-L., Harrop, B. E., Larson, V. E., Neale, R. B., Gettelman, A., Morrison, H., ... Leung, L. R. (2022, April). Better calibration of cloud parameterizations and subgrid effects increases the fidelity of the E3SM Atmosphere Model version 1. *Geoscientific Model Development*, *15*(7), 2881–2916. Retrieved 2023-05-12, from https://gmd.copernicus.org/articles/15/2881/2022/ doi: 10.5194/gmd-15-2881-2022

Margairaz, F., Pardyjak, E. R., & Calaf, M. (2020, October). Surface Thermal Heterogeneities and the Atmospheric Boundary Layer: The Thermal Heterogeneity Parameter. *Boundary-Layer Meteorology*, *177*(1), 49–68. Retrieved 2023-04-28, from https://link.springer.com/10.1007/s10546-020-00544-7 doi: 10.1007/s10546-020-00544-7

Maronga, B., & Raasch, S. (2013, January). Large-Eddy Simulations of Surface Heterogeneity Effects on the Convective Boundary Layer During the LITFASS-2003 Experiment. *Boundary-Layer Meteorology*, *146*(1), 17–44. Retrieved 2023-04-23, from http://link.springer.com/10.1007/s10546-012-9748-z doi: 10.1007/s10546-012-9748-z

Miller, S. T. K., Keim, B. D., Talbot, R. W., & Mao, H. (2003, September). Sea breeze: Structure, forecasting, and impacts: SEA BREEZE. *Reviews of Geophysics*, *41*(3). Retrieved 2023-04-23, from http://doi.wiley.com/10.1029/2003RG000124 doi: 10.1029/2003RG000124

Mitchell, K. E. (2004). The multi-institution North American Land Data Assimilation System (NLDAS): Utilizing multiple GCIP products and partners in a continental distributed hydrological modeling system. *Journal of Geophysical Research*, *109*(D7), D07S90. Retrieved 2023-05-12, from http://doi.wiley.com/10.1029/2003JD003823 doi: 10.1029/2003JD003823

Morrison, H., Curry, J. A., & Khvorostyanov, V. I. (2005, June). A New Double-Moment Microphysics Parameterization for Application in Cloud and Climate Models. Part I: Description. *Journal of the Atmospheric Sciences*, *62*(6), 1665–1677. Retrieved 2023-05-12, from https://journals.ametsoc.org/doi/10.1175/JAS3446.1 doi: 10.1175/JAS3446.1

Naumann, A. K., Stevens, B., & Hohenegger, C. (2019, May). A Moist Conceptual Model for the Boundary Layer Structure and Radiatively Driven Shallow Circulations in the Trades. *Journal of the Atmospheric Sciences*, *76*(5), 1289–1306. Retrieved 2023-05-11, from https://journals.ametsoc.org/doi/10.1175/JAS-D-18-0226.1 doi: 10.1175/JAS-D-18-0226.1

Naumann, A. K., Stevens, B., Hohenegger, C., & Mellado, J. P. (2017, October). A Conceptual Model of a Shallow Circulation Induced by Prescribed Low-Level Radiative Cooling. *Journal of the Atmospheric Sciences*, *74*(10), 3129–3144. Retrieved 2023-04-23, from https://journals.ametsoc.org/doi/10.1175/JAS-D-17-0030.1 doi: 10.1175/JAS-D-17-0030.1

Nilsson, J., & Emanuel, K. A. (1999, July). Equilibrium atmospheres of a two-column radiative-convective model. *Quarterly Journal of the Royal Meteorological Society*, *125*(558), 2239–2264. Retrieved 2023-04-28, from https://onlinelibrary.wiley.com/doi/10.1002/qj.49712555814 doi: 10.1002/qj.49712555814

Nuijens, L., & Emanuel, K. (2018, October). Congestus modes in circulating equilibria of the tropical atmosphere in a two-column model. *Quarterly Journal of the Royal Meteorological Society*, *144*(717), 2676–2692. Retrieved 2023-05-11, from https://onlinelibrary.wiley.com/doi/10.1002/qj.3385 doi: 10.1002/qj.3385

Raasch, S., & Harbusch, G. (2001, October). An Analysis Of Secondary Circulations And Their Effects Caused By Small-Scale Surface Inhomogeneities Using Large-Eddy Simulation. *Boundary-Layer Meteorology*, *101*(1), 31–59. Retrieved 2023-04-28, from http://link.springer.com/10.1023/A:

1019297504109 doi: 10.1023/A:1019297504109

Raymond, D. J., & Zeng, X. (2000, October). Instability and large-scale circulations in a two-column model of the tropical troposphere. *Quarterly Journal of the Royal Meteorological Society*, *126*(570), 3117–3135. Retrieved 2023-04-28, from https://onlinelibrary.wiley.com/doi/10.1002/qj.49712657007 doi: 10.1002/qj.49712657007

Rochetin, N., Couvreux, F., & Guichard, F. (2017, January). Morphology of breeze circulations induced by surface flux heterogeneities and their impact on convection initiation: Breeze Circulations Induced by Surface Heterogeneities. *Quarterly Journal of the Royal Meteorological Society*, *143*(702), 463–478. Retrieved 2023-04-28, from https://onlinelibrary.wiley.com/doi/10.1002/qj.2935 doi: 10.1002/qj.2935

Santanello, J. A., Dirmeyer, P. A., Ferguson, C. R., Findell, K. L., Tawfik, A. B., Berg, A., ... Wulfmeyer, V. (2018, June). Land–Atmosphere Interactions: The LoCo Perspective. *Bulletin of the American Meteorological Society*, *99*(6), 1253–1272. Retrieved 2023-05-11, from https://journals.ametsoc.org/view/journals/bams/99/6/bams-d-17-0001.1.xml doi: 10.1175/BAMS-D-17-0001.1

Simon, J., & Chaney, N. (2021, May). *Data for: Semi-coupling of a Field-scale Resolving Land-surface Model and WRF-LES to Investigate the Influence of Land-surface Heterogeneity on Cloud Development.* Zenodo. Retrieved from https://doi.org/10.5281/zenodo.4741327 doi: 10.5281/zenodo.4741327

Simon, J. S., Bragg, A. D., Dirmeyer, P. A., & Chaney, N. W. (2021, October). Semi-Coupling of a Field-Scale Resolving Land-Surface Model and WRF-LES to Investigate the Influence of Land-Surface Heterogeneity on Cloud Development. *Journal of Advances in Modeling Earth Systems*, *13*(10). Retrieved 2023-04-23, from https://onlinelibrary.wiley.com/doi/10.1029/2021MS002602 doi: 10.1029/2021MS002602

Stoll, R., Gibbs, J. A., Salesky, S. T., Anderson, W., & Calaf, M. (2020, December). Large-Eddy Simulation of the Atmospheric Boundary Layer. *Boundary-Layer Meteorology*, *177*(2-3), 541–581. Retrieved 2023-04-23, from https://link.springer.com/10.1007/s10546-020-00556-3 doi: 10.1007/s10546-020-00556-3

Sušelj, K., Teixeira, J., & Chung, D. (2013, July). A Unified Model for Moist Convective Boundary Layers Based on a Stochastic Eddy-Diffusivity/Mass-Flux Parameterization. *Journal of the Atmospheric Sciences*, *70*(7), 1929–1953. Retrieved 2023-05-12, from https://journals.ametsoc.org/doi/10.1175/JAS-D-12-0106.1 doi: 10.1175/JAS-D-12-0106.1

Taylor, C. M., De Jeu, R. A. M., Guichard, F., Harris, P. P., & Dorigo, W. A. (2012, September). Afternoon rain more likely over drier soils. *Nature*, *489*(7416), 423–426. Retrieved 2023-05-11, from http://www.nature.com/articles/nature11377 doi: 10.1038/nature11377

Torres-Rojas, L., Vergopolan, N., Herman, J. D., & Chaney, N. W. (2022, December). Towards an Optimal Representation of Sub-Grid Heterogeneity in Land Surface Models. *Water Resources Research*, *58*(12). Retrieved 2023-05-12, from https://onlinelibrary.wiley.com/doi/10.1029/2022WR032233 doi: 10.1029/2022WR032233

van Heerwaarden, C. C., Mellado, J. P., & De Lozar, A. (2014, November). Scaling Laws for the Heterogeneously Heated Free Convective Boundary Layer. *Journal of the Atmospheric Sciences*, *71*(11), 3975–4000. Retrieved 2023-04-28, from https://journals.ametsoc.org/doi/10.1175/JAS-D-13-0383.1 doi: 10.1175/JAS-D-13-0383.1

Vial, J., Dufresne, J.-L., & Bony, S. (2013, December). On the interpretation of inter-model spread in CMIP5 climate sensitivity estimates. *Climate Dynamics*, *41*(11-12), 3339–3362. Retrieved 2023-05-11, from http://link.springer

.com/10.1007/s00382-013-1725-9 doi: 10.1007/s00382-013-1725-9

Waterman, T. (2023, June). *tswater/clubb_scripts: Waterman2023.* Zenodo. Retrieved from https://doi.org/10.5281/zenodo.8092420 doi: 10.5281/zenodo.8092420

Weaver, C. P. (2004, December). Coupling between Large-Scale Atmospheric Processes and Mesoscale Land–Atmosphere Interactions in the U.S. Southern Great Plains during Summer. Part I: Case Studies. *Journal of Hydrometeorology*, *5*(6), 1223–1246. Retrieved 2023-04-23, from http://journals.ametsoc.org/doi/10.1175/JHM-396.1 doi: 10.1175/JHM-396.1

Witte, M. K., Herrington, A., Teixeira, J., Kurowski, M. J., Chinita, M. J., Storer, R. L., ... Bacmeister, J. (2022, September). Augmenting the Double-Gaussian Representation of Atmospheric Turbulence and Convection via a Coupled Stochastic Multi-Plume Mass-Flux Scheme. *Monthly Weather Review*, *150*(9), 2339–2355. Retrieved 2023-06-28, from https://journals.ametsoc.org/view/journals/mwre/150/9/MWR-D-21-0215.1.xml doi: 10.1175/MWR-D-21-0215.1

Zhang, L., Poll, S., & Kollet, S. (2023, January). Large-eddy simulation of soil moisture heterogeneity-induced secondary circulation with ambient winds. *Quarterly Journal of the Royal Meteorological Society*, *149*(751), 404–420. Retrieved 2023-04-28, from https://onlinelibrary.wiley.com/doi/10.1002/qj.4413 doi: 10.1002/qj.4413